

Ag₂S Quantum Dots as an Infrared Excited Photocatalyst for Hydrogen Production

Weili Yu,^{†,‡} Jun Yin,[‡] Yuan Li,[‡] Bo Lai,[§] Tong Jiang,^{||} Yangyang Li,[⊥] Huiwen Liu,[#] Jiale Liu,[#] Chen Zhao,[†] Subhash C. Singh,[§] Jingsheng Chen,[⊥] Bin Lin,^{*,‡,‡,‡,‡,‡} Hicham Idriss,^{*,§,§,§} and Chunlei Guo^{*,†,§}

[†]The Guo China-US Joint Photonics Laboratory (GPL), State Key Laboratory of Applied Optics (SKLAO), Changchun Institute of Optics, Fine Mechanics and Physics (CIOMP), Chinese Academy of Sciences (CAS), Changchun 130033, P. R. China

[‡]Physical Science and Engineering Division and [§]SABIC-CRD, King Abdullah University of Science and Technology (KAUST), Thuwal 23955-6900, Saudi Arabia

[§]The Institute of Optics, University of Rochester, Rochester, New York 14627, United States

^{||}Department of Journal, Jilin University of Arts, Changchun 130021, P. R. China

[⊥]Department of Materials Science and Engineering, National University of Singapore, Singapore 117576, Singapore

[#]State Key Laboratory of Supramolecular Structure and Materials, College of Chemistry, Jilin University, Changchun 130012, P. R. China

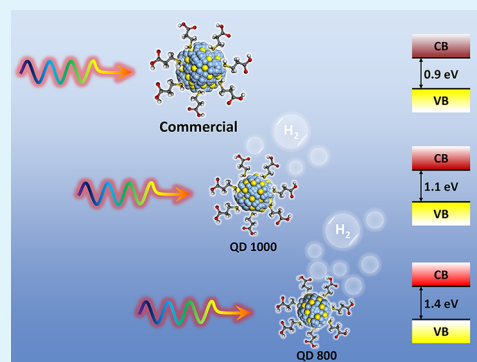
[‡]School of Energy Science and Engineering, University of Electronic Science and Technology of China, Chengdu 611731, P. R. China

[‡]Department of Chemistry, University College London, London WC1E 6BT, U.K.

Supporting Information

ABSTRACT: H₂ production using nanoscale semiconductors via photocatalytic water splitting is a much sought-after technology to curb carbon dioxide emission. Among the many challenges found to date is the search for a stable semiconductor photocatalyst responding to visible and preferably visible and IR light. Ag₂S is a narrow bandgap semiconductor with a bulk electronic gap smaller than that needed to split water. In this work, using a solvent thermal strategy, we have increased its bandgap energy by shifting up the conduction band edge to make it suitable for the electron transfer reaction to hydrogen ions. The Ag₂S quantum dots (QDs) were tested as both electrocatalysts and photocatalysts. As electrocatalysts, Ag₂S QDs with an absorption peak at 800 nm (QD800) showed the highest H₂ evolution activity with a Tafel slope of 89 mV/dec with an overpotential of 0.32 V. As photocatalysts, H₂ was produced at a rate of 858 μmol h⁻¹ g_{catal}⁻¹ under a white light flux of 100 mW cm⁻². Moreover, QD800 was also found to be active under only near-infrared excitation (800 ± 20 nm). This is the longest wavelength reported so far to excite a semiconductor and generate H₂.

KEYWORDS: photocatalysis, hydrogen evolution reaction, silver sulfide, near-infrared, quantum dots



INTRODUCTION

Molecular hydrogen production from non-fossil fuels is a much sought-after process to decrease CO₂ emission.^{1–3} Among the strategies developed for molecular hydrogen production, electrocatalytic and photocatalytic processes are the most promising ones, and considerable efforts have been devoted in the past decades in these directions. A large number of non-precious-metal-based wide bandgap semiconductors have been studied for this purpose, including transition metals, metal carbides, metal sulfides, and metal-free catalysts (e.g., C₃N₄).^{1–8} Research on narrow bandgap semiconductors is more limited.^{9–11} Yet, this is a crucial step to increase the solar to hydrogen conversion to a level that warrants application.

With a bulk bandgap of ca. 1 eV and negligible toxicity, Ag₂S has received attention for a variety of applications including solar cells,¹² photoconductors,¹³ bioimaging,¹⁴ and photocatalysts to reduce ions or degrade organic compounds.^{15–17} As photocatalysts for hydrogen evolution, some pioneering work has been conducted, and moderate hydrogen evolution rates were achieved. For example, Shen et al. reported that charge separation within Pt-loaded Ag₂S/CdS catalysts has enhanced their photocatalytic activity under simulated solar

Received: January 15, 2019

Accepted: March 12, 2019

Published: March 12, 2019

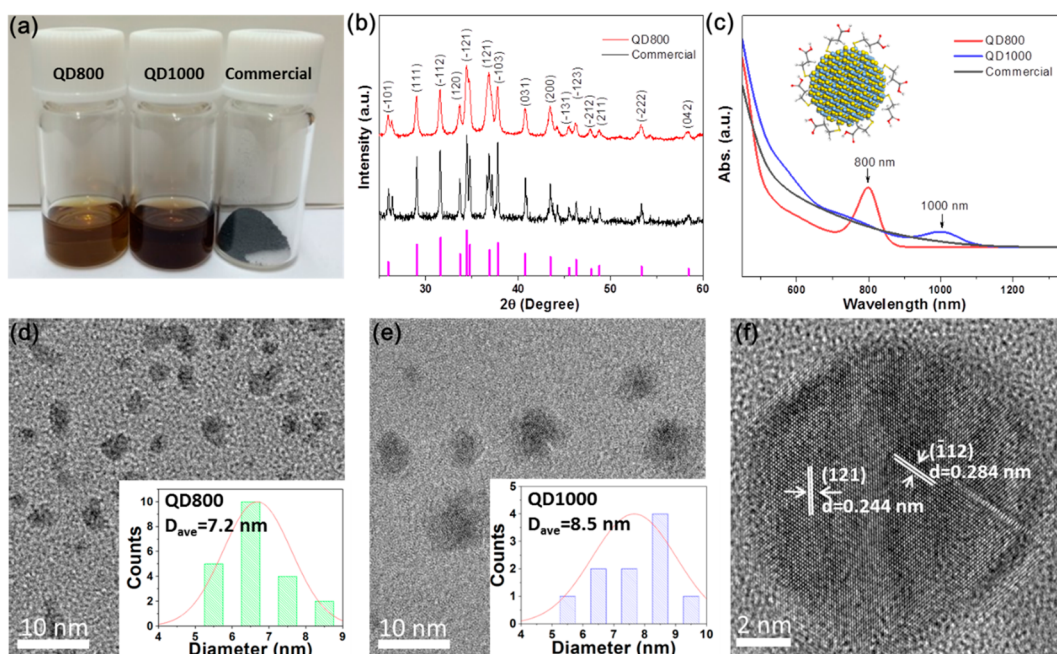


Figure 1. (a) Digital image of Ag_2S QDs in solutions and commercial Ag_2S . (b) XRD spectra of Ag_2S QDs and commercial Ag_2S . (c) UV-vis absorbance spectra of Ag_2S samples. TEM images of Ag_2S : (d) QD800 and (e) QD1000 samples. Insets: the distribution and average diameters of Ag_2S QDs. (f) HR-TEM image of an Ag_2S nanocrystal, which exhibits the hexagonal crystalline structure.

light (AM1.5).¹⁸ Sadovnikov et al. obtained a hydrogen production rate of $2.04 \mu\text{mol/h}$ under visible light irradiation (450 nm) using $\text{Ag}_2\text{S}/\text{Ag}$ heterostructure.¹⁹ Yu et al. synthesized and tested $\text{TiO}_2/\text{Ag}-\text{Ag}_2\text{S}$ photocatalysts and found a hydrogen production rate of $119 \mu\text{mol/h}$ under UV-light illumination.²⁰

The electrocatalytic activity of Ag_2S has also attracted considerable attention, and continuous progress has been made. Basu et al. synthesized $\text{Ag}_2\text{S}/\text{Ag}$ heterostructures and obtained a 200 mV overpotential at $10 \text{ mA}/\text{cm}^2$ current density, with a Tafel slope of $102 \text{ mV}/\text{dec}$.²¹ Further decreasing of the Tafel slope to $42 \text{ mV}/\text{dec}$ was reported by Wang et al. using $\text{Ag}_2\text{S}/\text{MoS}_2$ composites due to an enhanced charge separation.²² The intrinsic electrocatalytic and photocatalytic activities of Ag_2S nanocrystals were rarely reported to date.

Here we have found that semiconductor Ag_2S nanocrystals, when made with the right dimension and associated electronic bandgap, can be active electrocatalysts and photocatalysts for hydrogen ions reduction. These results may provide further insights into exploiting the working mechanism and the design of narrow bandgap semiconductor nanomaterials for photocatalysis.

EXPERIMENTAL SECTION

Synthesis of Ag_2S Quantum Dots. 0.17 g of AgNO_3 was dissolved in 50 mL of ethylene glycol (EG), and then 0.174 mL of 3-mercaptopropionic acid (MPA) was added. The mixture solution was bubbled with nitrogen for 10 min before heating to $145 \text{ }^\circ\text{C}$. The solution changed from transparent white to cloudy white and then to cloudy yellow. When the color was wine transparent, an aliquot of the solution was pumped away and characterized with a UV-vis spectrometer. Finally, the solution was cooled to room temperature. The resulting product was used for hydrogen evolution measurements with or without purification. Purified Ag_2S QDs were obtained by centrifuging the solution with anhydrous methanol for three times and dispersed in water or absolute ethanol.

Characterization and Testing. The crystal structure of Ag_2S QDs was identified by X-ray diffraction (XRD) (Bruker, D8 Advance). UV-vis spectra were recorded with Cary 100 Conc UV-vis spectrophotometer. The microstructure of the samples was characterized by TEM (Titan 80–300 kV (ST) TEM, FEI) equipped with X-ray energy dispersive spectroscopy (EDS). X-ray photoelectron spectra were measured using a Kratos Axis Ultra DLD spectrometer equipped with a monochromatic $\text{Al K}\alpha$ X-ray source ($h\nu = 1486.6 \text{ eV}$) operating at 150 W as well as a multichannel plate and a delay line detector under vacuum pressure of $1-10^{-9}$ mbar. Surface composition was determined using a pass energy of 20 eV and calibrated using adventitious carbon, C 1s, at 284.5 eV. Photocatalytic reactions were performed in a Pyrex reactor, and the gas amount was measured via an Agilent 7890A GC system. Ten milliliters of the in situ synthesized Ag_2S QDs and 15 mL of Na_2S (0.5 M) + Na_2SO_3 (0.5 M) aqueous solution were mixed together for hydrogen evolution measurements. To deposit Pd, 10 mM palladium(II) chloride aqueous solution was added into the above-mentioned mixture and was illuminated under a xenon lamp for half an hour before hydrogen evolution measurements. For photocatalytic experiments, a 300 W xenon lamp was used as a light source; 400 nm cutoff and 800 nm bandpass filters were utilized to achieve narrow-band light (full width at half-maximum equal 20 nm, as shown in the Supporting Information). The concentrations of Ag and S in the samples were determined via inductively coupled plasma optical emission spectrometry (ICP-OES) on a Varian 720-ES machine. The electrocatalytic experiments were performed on a standard three-electrode biologic electrochemical workstation (VMP3) connected to a rotating ring disk electrode (RRDE) apparatus. Ag_2S solution with 5 wt % Nafion 117 was dropped on the glassy carbon electrode (GCE) and dried in a vacuum chamber at $50 \text{ }^\circ\text{C}$ for half an hour. A graphite rod and Ag/AgCl (3.0 M KCl solution) worked as a counter electrode and a reference electrode, respectively. The CV, polarization curve, and Nyquist analyses were performed in 0.5 M H_2SO_4 aqueous solution with pH of 0.3. The potential was scanned between -0.8 and 0 V with modulated frequencies. To measure the flatband potentials, thin film electrodes of QDs and Commercial Ag_2S samples were fabricated on fluorine-doped tin oxide (FTO) conducting glasses by dropping the Ag_2S solution (with 5 wt % Nafion 117) on FTO and drying in air for 3 h. For commercial Ag_2S (from Sigma-Aldrich), the

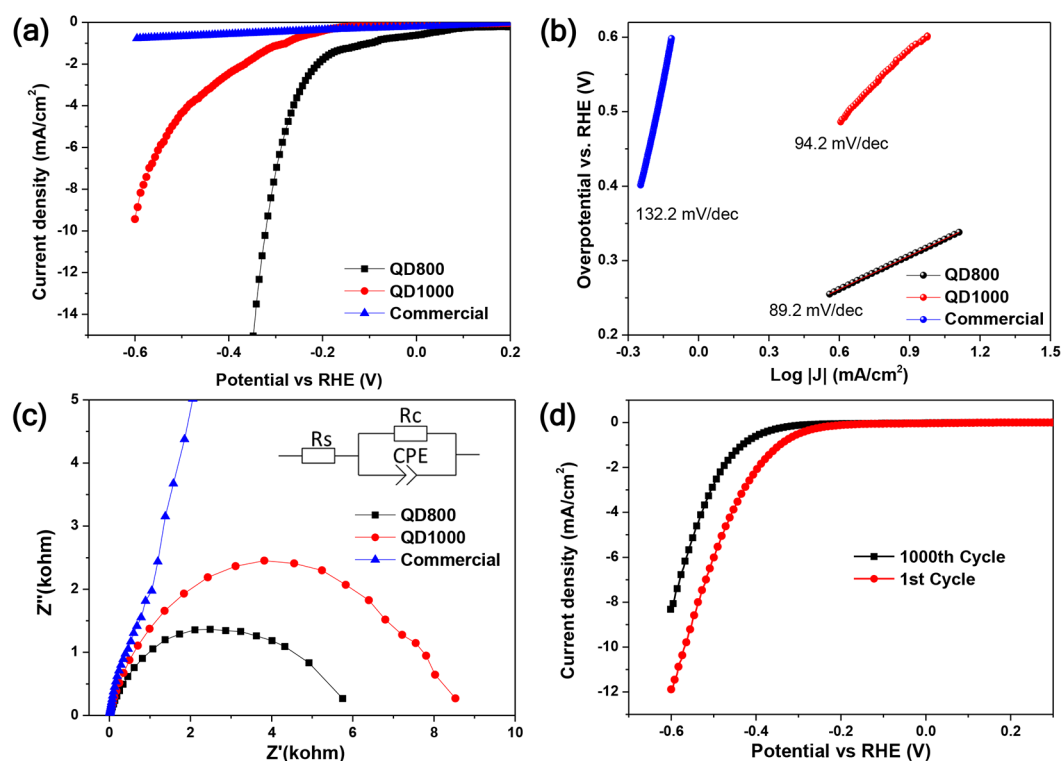


Figure 2. (a) Polarization curves, (b) corresponding Tafel plots, and (c) Nyquists plots of QD800, QD1000, and commercial Ag_2S crystals. The fitting equivalent circuit is shown as an inset, where R_s represents the uncompensated resistance, R_c represents the charge transfer resistance, and CPE represents the constant phase elements. (d) Stability test of the Ag_2S QD800 sample at the 1st cycle and after the 1000th cycle for HER.

powders were ball milled in DMF for 3 h. The electrochemical measurement was also conducted in a three-electrode cell. A Pt wire was used as counter electrode; Ag/AgCl (3.0 M KCl solution) electrode was used as a reference and Ag_2S QDs on FTO as a working electrode. The electrolyte was 0.4 M Na_2SO_4 solution (pH 6.8) deaerated by bubbling N_2 for half an hour before each experiment.

Computational Methods. Density functional theory (DFT) calculations were performed to optimize the crystal structure of β -phase Ag_2S by using the general gradient approximation (GGA)/Perdew–Burke–Ernzerhof (PBE) functional as implemented in the Quantum Espresso code.²³ The experimental crystal structure of β -phase Ag_2S at room temperature was used as an initial structure. Ultrasoft pseudopotentials were used to describe electron–ion interactions with electronic orbitals for S ($3s^2, 3p^4$) and Ag ($4s^2, 4p^6, 4d^{10}$), and plane-wave basis set cutoffs of the wave functions and the augmented density were set to be 50 and 300 Ry, respectively. The bulk crystal structure was fully relaxed until the total force on each atom was $<10^{-3}$ Ry/ \AA^{-1} . The Ag_2S QDs structures were cut from a large crystal with the consideration of both structural symmetry and ratio of Ag:S (2:1) atoms. The same computational methods were used to obtain the optimized structures and energy bandgaps of Ag_2S QDs with the size of 1.0–3.0 nm. The molecular graphics viewer (VESTA) was used to plot molecular structures and charge densities.

RESULTS AND DISCUSSION

Two synthesized Ag_2S QDs samples and a commercial Ag_2S micropowder (labeled as Commercial) are presented in Figure 1a. The QDs samples were dispersed in ethylene glycol (EG), and the commercial Ag_2S was a solid powder micrometers in size. The synthesized QDs with their first excitonic absorbance peaks at 800 and 1000 nm are labeled as Ag_2S QD800 and Ag_2S QD1000, respectively. XRD of Ag_2S QD800 and commercial Ag_2S are shown in Figure 1b; both exhibit a

monoclinic structure (β -phase).²⁴ The increased full width at half-maximum (fwhm) of the diffraction lines of QD800 is due to the decreased crystallite size. Figure 1c presents the UV–vis absorbance of the different samples. The absorbance onsets are at 860 and 1110 nm for QD800 and QD1000, respectively, from which the bandgaps are obtained (1.44 and 1.12 eV, respectively). Figures 1d and 1e present TEM images of the as-synthesized Ag_2S QD800 and Ag_2S QD1000, with their size distribution as shown in the inset. The Ag_2S QDs are nearly spherical in shape, with mean sizes of 7.2 and 8.5 nm for QD800 and QD1000, respectively. The QDs size and distribution can be tuned in a wider range;²⁵ here we focus on the samples QD800 and QD1000. A high-resolution TEM (HRTEM) image of an Ag_2S nanocrystal is shown in Figure 1f, in which the crystalline structure of Ag_2S QDs is seen. d spacings of 0.244 and 0.284 nm correspond to the interplanar spacing of the (121) and ($1\bar{1}2$), respectively. The energy-dispersive X-ray (EDX) spectrum shown in Figure S1 indicates that the QDs are composed of Ag and S elements only. From the ratio of Ag:S, S is found to be in excess, plausibly because of the S in the 3-mercaptopropionic acid (MPA) ligands. Therefore, the concentration of Ag_2S was calculated based on the amount of Ag.

The electrocatalytic activity of Ag_2S samples for the HER is displayed in Figure 2. Polarization curves of QD800, QD1000, and commercial (bulk) Ag_2S nanoparticles at a scan rate of 10 mV/s are shown in Figure 2a. The onset potentials (at a current density of 0.5 mA/cm^2) are 0.03, -0.21 , and -0.34 V for QD800, QD1000, and bulk Ag_2S samples, respectively. The overpotential (at the current density -10 mA/cm^2) of QD800 is at -0.32 V, much lower than that of QD1000 at ca. -0.6 V. For the commercial Ag_2S , the electrocatalytic activity was

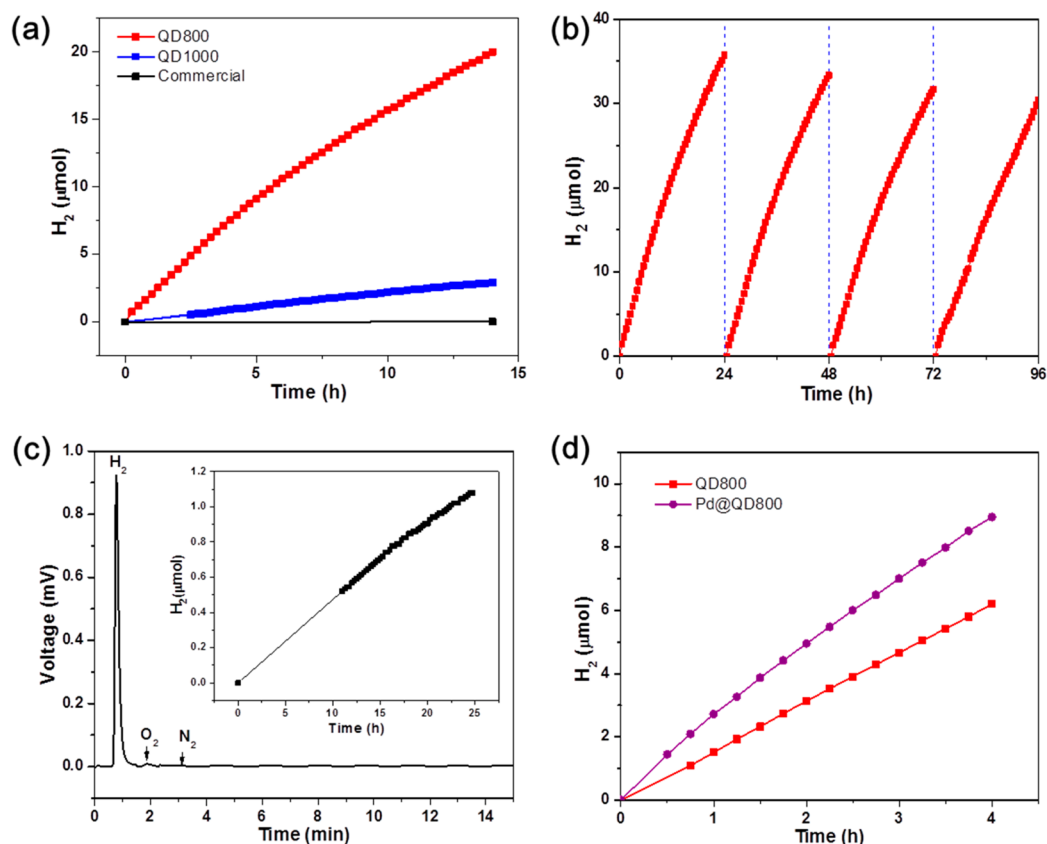


Figure 3. Photocatalytic performance. (a) Photocatalytic H₂ evolution over Ag₂S QD800, Ag₂S QD1000, and commercial Ag₂S. (b) Stability tests for Ag₂S QD800s dots. (c) Typical GC trace of H₂ evolution over Ag₂S QD800 under 800 nm excitation (± 20 nm); inset: H₂ evolution performance for 24 h. (d) H₂ evolution for Ag₂S QD800 with and without 1 wt % Pd. Light source: (a, b, d) white light (100 mW/cm²); (c) 800 \pm 20 nm light. Reaction conditions: 2.66 mg of Ag₂S QD in 10 mL of ethylene glycol, 15 mL of aqueous solution (0.5 M Na₂S and 0.5 M Na₂SO₃), pH = 12.4.

found to be far lower than that of the QDs and could not be measured. From the polarization curves, Tafel plots were obtained as shown in Figure 2b. For QD800, QD1000, and commercial Ag₂S nanoparticles, the Tafel slopes were found to be 89, 94, and 132 mV/dec, respectively. Furthermore, we have conducted electrochemical impedance spectroscopy (EIS) with frequencies varied from 10 mHz to 1 MHz and the Nyquist plots of the three samples as depicted in Figure 2c. The impedances of QD800 (11.34 k Ω), QD1000 (14.44 k Ω), and commercial Ag₂S indicate that QD800 has HER kinetics superior to QD1000 with a faster Faradaic process,^{26,27} which matches well with the polarization curves as shown in Figures 2a,b. The stability of the QD800 sample (Figure 2d) was investigated; the current density decreased to around 70% after 1000 cycles, which is comparable to other electrocatalytic semiconductors like CdS or CdSe.^{28–30}

To test the photocatalytic hydrogen evolution over Ag₂S QDs, the as-prepared 10 mL Ag₂S QDs solution in EG was added into an aqueous solution of Na₂S/Na₂SO₃ (15 mL, Na₂S 0.5 M, Na₂SO₃ 0.5 M). The sacrificial reagent S²⁻-containing solution was used to protect Ag₂S from oxidation.³¹ Figure 3 shows the photocatalytic performance of the Ag₂S samples. H₂ evolution curves upon illumination of white light (containing visible and infrared light from a xenon lamp) are shown in Figure 3a. The Ag₂S QD800 showed the highest H₂ evolution rate of 596 $\mu\text{mol h}^{-1} \text{g}_{\text{catal}}^{-1}$, which was much higher than that of Ag₂S QD1000 (55 $\mu\text{mol h}^{-1} \text{g}_{\text{catal}}^{-1}$). The commercial Ag₂S was not active. The difference in the H₂

evolution rates can be related to different energy levels and associated electron transfer ability due to the quantum confinement effect.^{28,32} The H₂ production rates mentioned above were obtained without a noble metal cocatalyst. This indicates that the photocatalyst is intrinsically active for hydrogen ions reduction, which is comparable with other metal sulfides or selenides, such as CdS and CdSe.^{28–30,33} It is worth mentioning that the Ag₂S QD samples aggregate when the EG solution of Ag₂S QDs was added into the alkaline solution (pH = 12.4). This might be due to the electrostatic interactions between the MPA capping Ag₂S QDs and medium ions.³⁴ The aggregation was, however, less pronounced after sonication. As shown in Figure 3b, H₂ evolution rates decreased by ca. 16% after 96 h. To further see the activity of Ag₂S QDs under long wavelength illumination, a narrow-band light with a wavelength centered at 800 nm (800 \pm 20 nm; flux 3.67 mW/cm², Figure S2) was used (Figure 3c). From TEM images, assuming the 800 nm sized QDs are spherical and with a radius of 7.2 nm, the hydrogen produced per mole of Ag₂S QDs per hour can be calculated. After 24 h, 2.66 mg of Ag₂S QD800 produced 1.06 μmol of H₂, corresponding to 16.6 $\mu\text{mol h}^{-1} \text{g}_{\text{catal}}^{-1}$, indicating that Ag₂S QD800 was active upon excitation with IR light. Under illumination of white light (100 mW/cm²), this system achieved a turnover number (TON) of 506 (defined as moles of H₂ per mole of QDs) after 12 h.

Transition metals with work function higher than that of a semiconductor can help to trap excited electrons and in turn reduce hydrogen ions to hydrogen molecules.^{31,33} Photo-

Table 1. Concentration of Ag₂S QDs in Ethylene Glycol Solution and the H₂ Evolution Rates of Ag₂S Samples under 100 mW/cm² Illumination

samples	abs onset (nm)	E _g (eV)	Ag ^a (mol/mL)	S ^a (mol/mL)	Ag ₂ S (mg/10 mL)	H ₂ (μmol g _{catal} ⁻¹ h ⁻¹)
QD800	860	1.44	2.148	1.47	2.66	596
QD1000	1110	1.12	2.907	11.03	3.61	55
Commercial	1370	0.91		7.20	0.4 ^b	0

^aConcentration was measured by ICP. ^bCommercial Ag₂S was nondispersible in aqueous solution.

deposition of Pd on Ag₂S QDs surface was thus prepared and tested for H₂ evolution. As shown in Figure 3d, the Pd/Ag₂S QD800 catalyst showed ca. 1.5 times increase in activity, reaching 858 μmol g_{catal}⁻¹ h⁻¹. The role for Pd enhancement may be attributed to two effects. First, Pd particles on Ag₂S surface may serve as electron collectors and provide reduction sites, thus decreasing the carriers' recombination rates.³⁵ Second, the Pd²⁺ ions from palladium(II) chloride might react with the S²⁻ ions and form PdS which may contribute into the reaction rate.²⁹ The effect of organic solvent, EG, on H₂ evolution was also investigated. Removing the EG was made by centrifugation and redispersion of Ag₂S QD800 in aqueous solution. Hydrogen evolution rate was then measured and found to be equal 54 μmol g_{catal}⁻¹ h⁻¹. This is about one-tenth of that found in the presence of EG as shown in Figure S3. In the absence of EG a considerable particle agglomeration has taken place, and this might be the reason for the sharp drop in activity. It is also possible that EG acts as a hole trap.³⁶ Hole trapping compounds were previously found to enhance

the reaction rates even in the presence of S²⁻ ions in the case of Au/CdS.³⁷

We have then studied the possible changes of the elemental composition and oxidation state of Ag₂S QDs before and after photocatalysis by XPS (Figure 4). The binding energy was calibrated with respect to C 1s (284.5 eV). The binding energies of the silver 3d lines of the as-prepared catalyst were found to be at 367.7 and 373.7 eV. Both the binding energy position and associated spin-orbit splitting are consistent with those of 3d_{5/2} and 3d_{3/2} of Ag⁺ cations in Ag₂S.³⁸ XPS core level lines of Ag metal and its oxides (Ag₂O and AgO) have been studied in good detail for decades. The main characteristic is "unusual" negative shift in the binding energy when metal silver is oxidized. This uncommon shift, due to changes in work function and extra atomic relaxation, has been discussed in details elsewhere.³⁹ After photocatalytic reaction for 96 h, a binding energy shift of 0.4 eV was observed. This indicates that the surface of Ag₂S may contain Ag atoms in their metallic state. For the S 2p spectra, before photoreaction, the peaks at 162.1 and 160.9 eV are assigned to S 2p_{1/2} and S 2p_{3/2}, respectively.⁴⁰ After photoreaction, a slight increase in the fwhm of the S 2p line at ca. 162 eV is observed, most likely due to some oxidation of S ions. A quantitative analysis showed that the S/Ag atomic ratio changed slightly from 1/1.66 before reaction to 1/1.61 after reaction. This is close to the atomic ratio provided by the EDX spectrum and may be due to the fact that some S anions (from S²⁻ ions in the solution or from the MPA ligand) were oxidized during the photocatalytic reaction.^{31,41}

The dependence of hydrogen evolution on nanocrystal size can be quantitatively understood by Marcus theory,⁴² which supports the higher charge transfer rates at the interfaces of

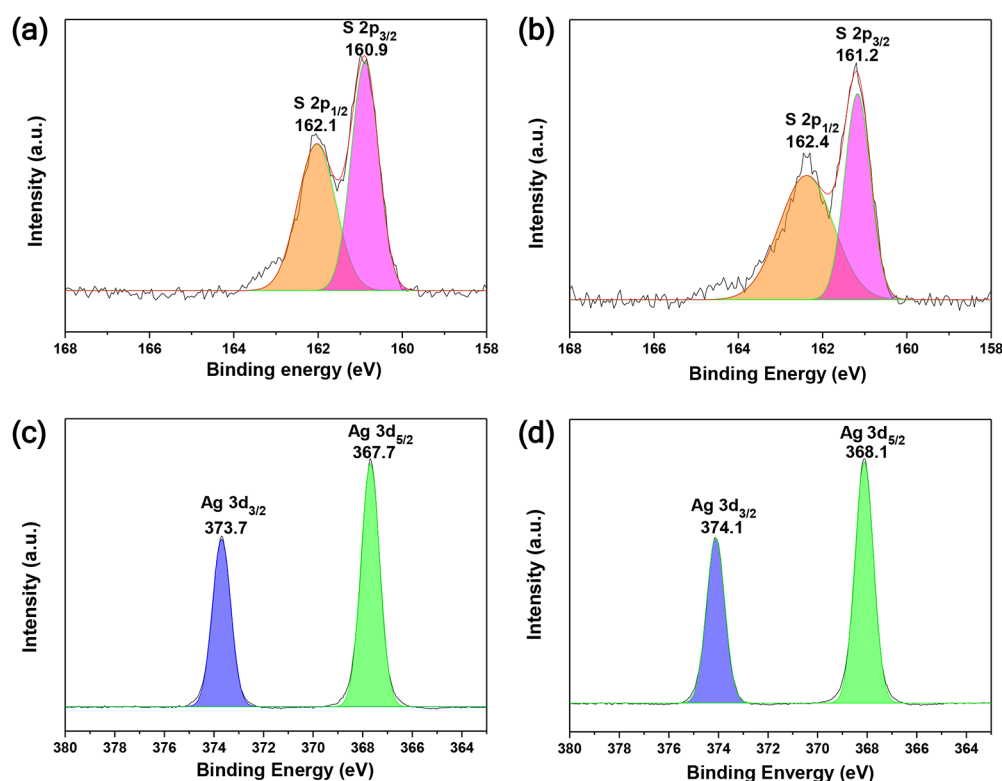


Figure 4. XPS spectra of S 2p and Ag 3d from Ag₂S QD800 measured before (a, c) and after (b, d) the photocatalytic reaction for 96 h.

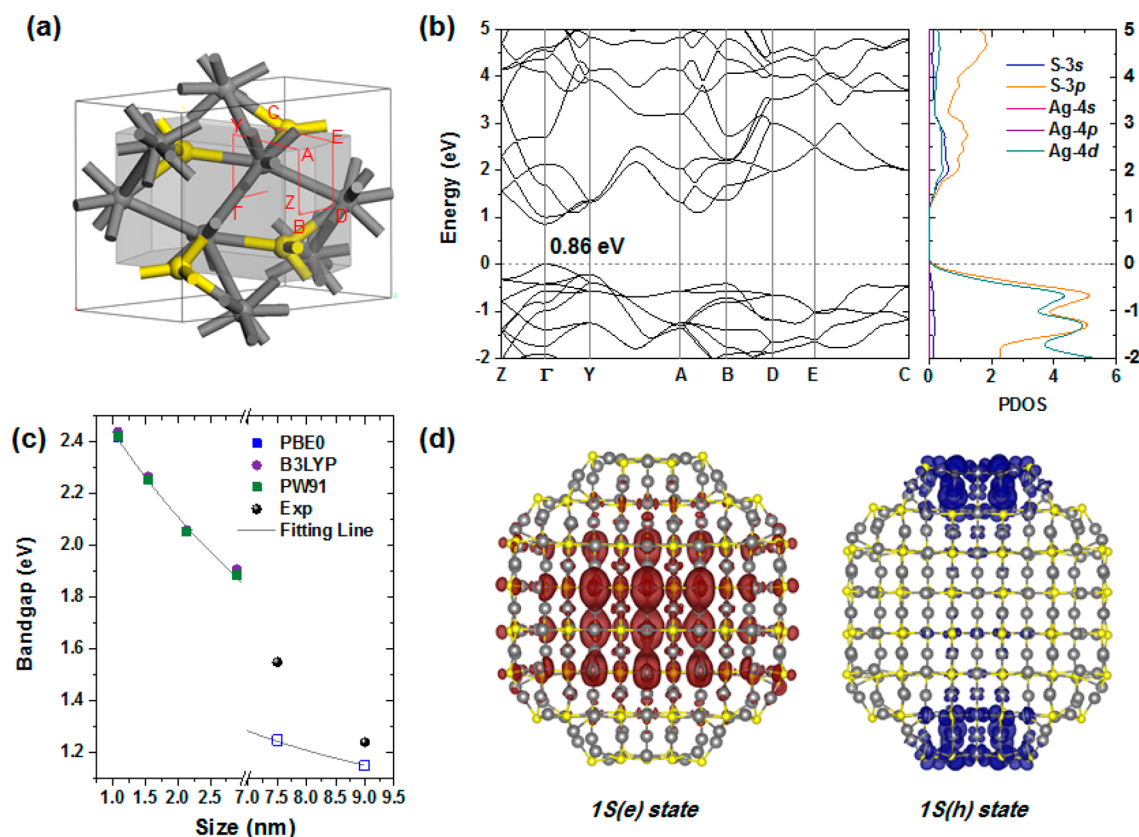


Figure 5. DFT-GGA-PBE computation. (a) Crystal structure (yellow are 4-fold coordinated S atoms and gray are 8-fold coordinated Ag atoms; the letters inside are related to reciprocal space vectors as indicated in part b). (b) GGA/PBE-calculated band structure and density of states of the bulk β -phase Ag_2S . (c) Calculated and extrapolated bandgaps of Ag_2S QDs with diameters in the range 1.0–9.0 nm as well as the experimental values of Ag_2S QD800 and QD1000. (d) Charge density of 1S state for LUMO (left panel) and HOMO (right panel) of Ag_2S QD (2.91 nm).

smaller nanocrystals due to improved thermodynamics.^{28,32,43,44} To further probe into the electronic structure of Ag_2S , we have performed density functional theory (DFT) of the Ag_2S QDs and bulk (Figure 5). Figure 5a shows the structure of Ag_2S QD without ligand, where Ag atoms are 8-fold coordinated while S atoms are 4-fold coordinated. As seen from Figure 5b, the calculated band structure of the bulk β -phase of Ag_2S has a direct bandgap of 0.86 eV at the Γ -point, slightly smaller than the experimental value of 0.95 eV deduced from the absorption spectra displayed in Figure 1c. To explore the size effect, we have calculated the bandgap of Ag_2S QDs with sizes in the range of 1.0–3.0 nm and extrapolated the bandgaps of larger QDs by fitting the calculated data, as shown in Figure 5c. The bandgaps of Ag_2S QD800 and QD1000 obtained by the fitting procedure are 1.25 and 1.15 eV, respectively. While these values are smaller than the corresponding experimental data, similar behavior of exponential decay has been observed when increasing the size of the QDs as a result of strong quantum confinement effects.^{23,41} We have performed similar computation work using the HF-DFT hybrid method (B3LYP), and the extracted bandgaps were found to be similar to those obtained using pure DFT (PBE0) (Table S1). The difference between the calculated and experimental results might also be due to surface states of the QDs of our model, in which the dangling bonds on the surface of the QDs are not passivated by the ligands for the sake of computational cost. We have also calculated the charge density of the Ag_2S QDs with diameter of 2.91 nm (Figure 5d). The HOMO is delocalized with high contribution of S 3p

orbitals at the central region of the QD while the LUMO is localized on both S 3p and Ag 4d at two edges of the cluster.

To further probe into the potential of Ag_2S QDs as a narrow bandgap semiconductor for water reduction to hydrogen, we conducted Mott–Schottky analysis, from which the flatband potentials and carrier densities were obtained. The Mott–Schottky equation is

$$\frac{1}{C_{\text{sc}}^2} = \frac{2}{\epsilon_0 \epsilon_r e N_D A^2} \left(\phi_A - \phi_{\text{FB}} - \frac{kT}{e} \right)$$

where the C_{sc} is the capacitance of the space charge and ϵ_0 and ϵ_r are the absolute and relative dielectric constants, respectively. The constant A is the area, while N_D is the concentration of donors. ϕ_A and ϕ_{FB} are the applied potential and flatband potential, respectively. On the basis of the positive Mott–Schottky slopes, the samples demonstrated their characteristic n-type character. By plotting $1/C_{\text{sc}}^2$ as a function of the applied potential ϕ_A , the value of the flatband potential ϕ_{FB} is obtained from the intercept on the potential axis. The carrier concentrations used for the calculation are taken as $1.82 \times 10^{14}/\text{cm}^3$ and $4.67 \times 10^{15}/\text{cm}^3$ for QD 800 and QD1000, respectively. The Mott–Schottky plots for the different Ag_2S QD samples are shown in Figures 6a to c. The ϕ_{FB} values for QD800, QD1000, and bulk Ag_2S materials are extracted as -0.175 , 0.015 , and 0.03 V, respectively. As ϕ_{FB} reflects the potential that needs to be applied to the Ag_2S to reduce the band bending to zero, it indicates that QD800 can reduce water without applied potential. Considering that the ϕ_{FB} denotes the Fermi level position of semiconductor with

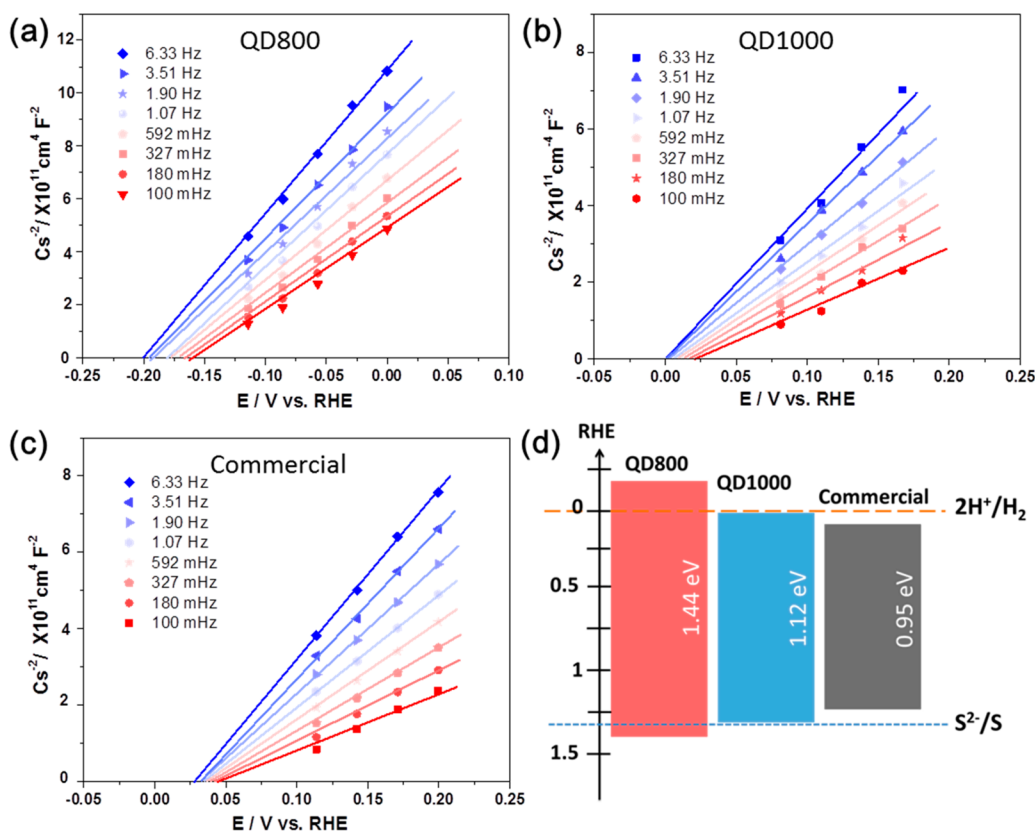


Figure 6. Mott–Schottky plots for Ag_2S samples of (a) QD800, (b) QD1000, and (c) commercial Ag_2S , respectively. The flatband potentials are obtained from the intercepts of the extrapolated lines with the x -axis. (d) Band alignments of Ag_2S QDs and commercial Ag_2S .

respect to the potential of the reference electrode and that the ϕ_{FB} value obtained for QD1000 is within the conduction band edges, we infer that it may reduce water to hydrogen while bulk Ag_2S is not active for water reduction. The energy level positions, Fermi levels and water-reduction potentials are presented in Figure 6d. The electrocatalytic and photocatalytic activity is attributed to a quantum confinement effect, which depends on the nanocrystal size and in turn affects the energy alignments of the crystals, as well as the charge transfer across the interfaces.^{28,45}

The challenge in developing stable and active narrow bandgap photocatalyst lies in both thermodynamic and kinetic grounds. The electrocatalytic results showed that Ag_2S QD800 is kinetically favorable, as shown in Figure 2, while Figures 5 and 6 give further evidence that when the size of Ag_2S QDs decreases, thermodynamic considerations are satisfied. Some pioneering works were conducted aiming at narrow bandgap materials. For example, it was reported that BaZrO_3 – BaTaO_2N solid solutions were capable of both photocatalytically reduce and oxidize water under light irradiation above 660 nm.⁹ It was further demonstrated that BaNbO_2N can be activated for the photocatalytic water oxidation and reduction in the presence of sacrificial agents under light illumination up to 740 nm.¹¹ Results of the present work are a further step in this direction extending light absorption to 800 nm.

It is worth mentioning that solar to hydrogen efficiency of at least 10% is needed for a practical photocatalytic system to occur.^{46,47} The complete system will eventually be composed of a multiphase semiconductor system where light is absorbed in the UV, visible, and near-IR regions, sequentially. This system already exists in multijunction solar cells⁴⁷ and is

presently pursued as a photocatalyst panel for hydrogen evolution.⁴⁸ Although it is unclear which system will prevail, pursuing research in these directions would ultimately provide the needed energy from solar by nanomaterials. The possibility of utilizing Ag_2S to harvest light in the IR and visible light while making molecular hydrogen may find its use in a hybrid solar–photo cells. For example, it can be deposited or grown on the surface of multijunction cells benefiting from their fast electron/hole transfer rate and thus preventing its corrosion and allowing at the same time enhancement of cell efficiency. Because of the simplicity of the synthetic method, they can be dispersed in solvents and fabricated into thin films. Another key observation is that quantum size effect can change the balance between the input and output, i.e., more light absorbed and less energy wasted. In other words, they can be tuned to match both the band energies and bend edges so alignment with other semiconductors is made possible for both hydrogen and oxygen productions.

CONCLUSIONS

The solvothermal method synthesized Ag_2S QDs with MPA ligands for hydrogen production was investigated. Ag_2S QDs are found to be active electrocatalysts with a Tafel slope of 89 mV/dec and an overpotential of 0.32 V. As photocatalysts, the Pd/ Ag_2S QD800 had a hydrogen evolution rate of ca. 850 $\mu\text{mol h}^{-1} \text{g}^{-1}$. In addition, Ag_2S QDs can harvest a large fraction of solar light extending to the NIR region, here confirmed to be ~ 800 nm, one of the largest wavelength reported for photocatalysis so far. The variability in electrocatalytic and photocatalytic performance was found due to their tunable size-induced quantum confinement effect.

■ ASSOCIATED CONTENT

Supporting Information

The Supporting Information is available free of charge on the ACS Publications website at DOI: 10.1021/acsae.9b00091.

Light source spectra, EDS analysis, hydrogen production curve, DFT-computed bandgaps of Ag₂S QDs, literature survey of photocatalysts and hydrogen evolution reactions based on Ag₂S (PDF)

■ AUTHOR INFORMATION

Corresponding Authors

*E-mail guo@ciomp.ac.cn.

*E-mail h.idriss@ucl.ac.uk.

*E-mail bin@mail.ustc.edu.cn.

ORCID

Weili Yu: 0000-0001-5075-9638

Jun Yin: 0000-0002-1749-1120

Jingsheng Chen: 0000-0003-3188-2803

Hicham Idriss: 0000-0001-8614-7019

Author Contributions

W.Y., B.L., and H.I. conceived the project. W.Y. and C.Z. fabricated Ag₂S samples. J.Y. and Y.L. performed the DFT calculations. T.J., Y.L. J.C., and S.S. helped with the data collection and analysis. B.L. and C.Z. conducted electrochemical measurements. W.Y. and B.L. did the photocatalysis experiments; C.G., H.I., and B.L. oversaw the project. W.Y., H.I., and B.L. wrote the manuscript. All authors discussed and commented on the manuscript.

Notes

The authors declare no competing financial interest.

■ ACKNOWLEDGMENTS

This work was supported by National Natural Science Foundation of China (91750205, 61774155, 51102107, 91750205, and 21404015) and the National Key R & D Program of China (2017YFB1104700).

■ REFERENCES

- (1) Fox, M. A.; Dulay, M. T. Heterogeneous Photocatalysis. *Chem. Rev.* **1993**, *93*, 341–357.
- (2) Asahi, R.; Morikawa, T.; Ohwaki, T.; Aoki, K.; Taga, Y. Visible-light Photocatalysis in Nitrogen-doped Titanium Oxides. *Science* **2001**, *293*, 269–271.
- (3) Wang, J.; Xu, F.; Jin, H.; Chen, Y.; Wang, Y. Non-Noble Metal-based Carbon Composites in Hydrogen Evolution Reaction: Fundamentals to Applications. *Adv. Mater.* **2017**, *29*, 1605838.
- (4) Pincella, F.; Isozaki, K.; Miki, K. A Visible Light-driven Plasmonic Photocatalyst. *Light: Sci. Appl.* **2014**, *3*, e133.
- (5) Gottlieb, E.; Kopeć, M.; Banerjee, M.; Mohin, J.; Yaron, D.; Matyjaszewski, K.; Kowalewski, T. In-Situ Platinum Deposition on Nitrogen-Doped Carbon Films as a Source of Catalytic Activity in a Hydrogen Evolution Reaction. *ACS Appl. Mater. Interfaces* **2016**, *8*, 21531–21538.
- (6) Huang, H.; Huang, J.; Liu, W.; Fang, Y.; Liu, Y. Ultradispersed and Single-Layered MoS₂ Nanoflakes Strongly Coupled with Graphene: An Optimized Structure with High Kinetics for the Hydrogen Evolution Reaction. *ACS Appl. Mater. Interfaces* **2017**, *9*, 39380–39390.
- (7) Wu, C.; Li, J. Unique Hierarchical Mo₂C/C Nanosheet Hybrids as Active Electrocatalyst for Hydrogen Evolution Reaction. *ACS Appl. Mater. Interfaces* **2017**, *9*, 41314–41322.

(8) Xie, A.; Xuan, N.; Ba, K.; Sun, Z. Pristine Graphene Electrode in Hydrogen Evolution Reaction. *ACS Appl. Mater. Interfaces* **2017**, *9*, 4643–4648.

(9) Maeda, K.; Domen, K. Water Oxidation Using a Particulate BaZrO₃-BaTaO₂N Solid-Solution Photocatalyst That Operates under a Wide Range of Visible Light. *Angew. Chem., Int. Ed.* **2012**, *51*, 9865–9869.

(10) Ishikawa, A.; Takata, T.; Kondo, J. N.; Hara, M.; Kobayashi, H.; Domen, K. Oxysulfide Sm₂Ti₂S₂O₅ as a Stable Photocatalyst for Water Oxidation and Reduction under Visible Light Irradiation ($\lambda \leq 650$ nm). *J. Am. Chem. Soc.* **2002**, *124*, 13547–13553.

(11) Hisatomi, T.; Katayama, C.; Moriya, Y.; Minegishi, T.; Katayama, M.; Nishiyama, H.; Yamada, T.; Domen, K. Photocatalytic Oxygen Evolution using BaNbO₂N Modified with Cobalt Oxide under Photoexcitation up to 740 nm. *Energy Environ. Sci.* **2013**, *6*, 3595–3599.

(12) Bruhwiler, D.; Leiggner, C.; Glaus, S.; Calzaferri, G. Luminescent Silver Sulfide Clusters. *J. Phys. Chem. B* **2002**, *106*, 3770–3777.

(13) Hull, S.; Keen, D. A.; Sivia, D. S.; Madden, P. A.; Wilson, M. The High-temperature Superionic Behaviour of Ag₂S. *J. Phys.: Condens. Matter* **2002**, *14*, L9–L17.

(14) Hong, G.; Robinson, J. T.; Zhang, Y.; Diao, S.; Antaris, A. L.; Wang, Q.; Dai, H. In Vivo Fluorescence Imaging with Ag₂S Quantum Dots in the Second Near-Infrared Region. *Angew. Chem., Int. Ed.* **2012**, *51*, 9818–9821.

(15) Yang, W.; Zhang, L.; Hu, Y.; Zhong, Y.; Wu, H. B.; Lou, X. W. Microwave-assisted Synthesis of Porous Ag₂S-Ag hybrid Nanotubes with High Visible-light Photocatalytic Activity. *Angew. Chem., Int. Ed.* **2012**, *51*, 11501–11504.

(16) Wang, X.; Zhan, S.; Wang, Y.; Wang, P.; Yu, H.; Yu, J.; Hu, C. Facile Synthesis and Enhanced Visible-light Photocatalytic Activity of Ag₂S Nanocrystal-sensitized Ag₈W₄O₁₆ Nanorods. *J. Colloid Interface Sci.* **2014**, *422*, 30–37.

(17) Meng, Z.-D.; Ghosh, T.; Zhu, L.; Choi, J.-G.; Park, C.-Y.; Oh, W.-C. Synthesis of Fullerene Modified with Ag₂S with High Photocatalytic Activity under Visible Light. *J. Mater. Chem.* **2012**, *22*, 16127–16135.

(18) Shen, S.; Guo, L.; Chen, X.; Ren, F.; Mao, S. S. Effect of Ag₂S on Solar-driven Photocatalytic Hydrogen Evolution of Nanostructured CdS. *Int. J. Hydrogen Energy* **2010**, *35*, 7110–7115.

(19) Sadovnikov, S. I.; Kozlova, E. A.; Gerasimov, E. Y.; Rempel, A. A.; Gusev, A. I. Enhanced Photocatalytic Hydrogen Evolution from Aqueous Solutions on Ag₂S/Ag Heteronanostructure. *Int. J. Hydrogen Energy* **2017**, *42*, 25258–25266.

(20) Yu, H.; Liu, W.; Wang, X.; Wang, F. Promoting the interfacial H₂-evolution Reaction of Metallic Ag by Ag₂S Cocatalyst: A Case Study of TiO₂/Ag-Ag₂S Photocatalyst. *Appl. Catal., B* **2018**, *225*, 415–423.

(21) Basu, M.; Nazir, R.; Mahala, C.; Fageria, P.; Chaudhary, S.; Gangopadhyay, S.; Pande, S. Ag₂S/Ag Heterostructure: A Promising Electrocatalyst for the Hydrogen Evolution Reaction. *Langmuir* **2017**, *33*, 3178–3186.

(22) Wang, M.; Ju, P.; Li, W.; Zhao, Y.; Han, X. Ag₂S Nanoparticle-decorated MoS₂ for Enhanced Electrocatalytic and Photoelectrocatalytic Activity in Water Splitting. *Dalton Trans.* **2017**, *46*, 483–490.

(23) Giannozzi, P.; et al. Quantum Espresso: A Modular and Open-source Software Project for Quantum Simulations of Materials. *J. Phys.: Condens. Matter* **2009**, *21*, 395502.

(24) Jiang, P.; Zhu, C.-N.; Zhang, Z.-L.; Tian, Z.-Q.; Pang, D.-W. Water-soluble Ag₂S Quantum Dots for Near-infrared Fluorescence Imaging in vivo. *Biomaterials* **2012**, *33*, 5130–5135.

(25) Sahu, A.; Qi, L.; Kang, M. S.; Deng, D.; Norris, D. J. Facile Synthesis of Silver Chalcogenide (Ag₂E; E = Se, S, Te) Semiconductor Nanocrystals. *J. Am. Chem. Soc.* **2011**, *133*, 6509–6512.

(26) Zhang, Y.; Wang, Y.; Han, C.; Jia, S.; Zhou, S.; Zang, J. Tungsten-coated Nano-boron Carbide as a Non-noble Metal Bifunctional Electrocatalyst for Oxygen Evolution and Hydrogen

Evolution Reactions in Alkaline Media. *Nanoscale* **2017**, *9*, 19176–19182.

(27) Lai, Z.; Chaturvedi, A.; Wang, Y.; Tran, T. H.; Liu, X.; Tan, C.; Luo, Z.; Chen, B.; Huang, Y.; Nam, G.-H.; Zhang, Z.; Chen, Y.; Hu, Z.; Li, B.; Xi, S.; Zhang, Q.; Zong, Y.; Gu, L.; Kloc, C.; Du, Y.; Zhang, H. Preparation of 1T'-Phase $\text{ReS}_{2x}\text{Se}_{2(1-x)}$ ($x = 0-1$) Nanodots for Highly Efficient Electrocatalytic Hydrogen Evolution Reaction. *J. Am. Chem. Soc.* **2018**, *140*, 8563–8568.

(28) Zhao, J.; Holmes, M. A.; Osterloh, F. E. Quantum Confinement Controls Photocatalysis: A Free Energy Analysis for Photocatalytic Proton Reduction at CdSe Nanocrystals. *ACS Nano* **2013**, *7*, 4316–4325.

(29) Yan, H.; Yang, J.; Ma, G.; Wu, G.; Zong, X.; Lei, Z.; Shi, J.; Li, C. Visible-light-driven Hydrogen Production with Extremely High Quantum Efficiency on Pt-PdS/CdS Photocatalyst. *J. Catal.* **2009**, *266*, 165–168.

(30) Jin, J.; Yu, J.; Liu, G.; Wong, P. K. Single crystal CdS Nanowires with High Visible-light Photocatalytic H_2 -production Performance. *J. Mater. Chem. A* **2013**, *1*, 10927–10934.

(31) Yu, W.; Isimjan, T.; Del Gobbo, S.; Anjum, D. H.; Abdel-Azeim, S.; Cavallo, L.; Garcia-Esparza, A. T.; Domen, K.; Xu, W.; Takanabe, K. Tethering Metal Ions to Photocatalyst Particulate Surfaces by Bifunctional Molecular Linkers for Efficient Hydrogen Evolution. *ChemSusChem* **2014**, *7*, 2575–2583.

(32) Jasieniak, J.; Califano, M.; Watkins, S. E. Size-Dependent Valence and Conduction Band-Edge Energies of Semiconductor Nanocrystals. *ACS Nano* **2011**, *5*, 5888–5902.

(33) Dukovic, G.; Merkle, M. G.; Nelson, J. H.; Hughes, S. M.; Alivisatos, A. P. Photodeposition of Pt on Colloidal CdS and CdSe/CdS Semiconductor Nanostructures. *Adv. Mater.* **2008**, *20*, 4306–4311.

(34) Zhang, H.; Wang, D.; Yang, B.; Moehwald, H. Manipulation of Aqueous Growth of CdTe Nanocrystals to Fabricate Colloidally Stable One-dimensional Nanostructures. *J. Am. Chem. Soc.* **2006**, *128*, 10171–10180.

(35) Qian, K.; Sweeny, B. C.; Johnston-Peck, A. C.; Niu, W.; Graham, J. O.; DuChene, J. S.; Qiu, J.; Wang, Y.-C.; Engelhard, M. H.; Su, D.; Stach, E. A.; Wei, W. D. Surface Plasmon-Driven Water Reduction: Gold Nanoparticle Size Matters. *J. Am. Chem. Soc.* **2014**, *136*, 9842–9845.

(36) Al-Azri, Z. H. N.; Chen, W.-T.; Chan, A.; Jovic, V.; Ina, T.; Idriss, H.; Waterhouse, G. I. N. The Roles of Metal Co-catalysts and Reaction Media in Photocatalytic Hydrogen Production: Performance Evaluation of M/TiO₂ Photocatalysts (M = Pd, Pt, Au) in Different Alcohol–water Mixtures. *J. Catal.* **2015**, *329*, 355–367.

(37) Majeed, I.; Nadeem, M. A.; Al-Oufi, M.; Nadeem, M. A.; Waterhouse, G. I. N.; Badshah, A.; Metson, J. B.; Idriss, H. On the Role of Metal Particle Size and Surface Coverage for Photo-catalytic Hydrogen Production: A Case Study of the Au/CdS System. *Appl. Catal., B* **2016**, *182*, 266–276.

(38) Romand, M.; Roubin, M.; Deloume, J. P. ESCA Studies of Some Copper and Silver Selenides. *J. Electron Spectrosc. Relat. Phenom.* **1978**, *13*, 229–242.

(39) Weaver, J. F.; Hoflund, G. B. Surface Characterization Study of the Thermal Decomposition of AgO. *J. Phys. Chem.* **1994**, *98*, 8519–8524.

(40) Cova, C. M.; Zuliani, A.; Puente Santiago, A. R.; Caballero, A.; Muñoz-Batista, M. J.; Luque, R. Microwave-assisted Preparation of Ag/Ag₂S Carbon Hybrid Structures from Pig Bristles as Efficient HER Catalysts. *J. Mater. Chem. A* **2018**, *6*, 21516–21523.

(41) Yu, X.-R.; Liu, F.; Wang, Z.-Y.; Chen, Y. Auger Parameters for Sulfur-containing Compounds using a Mixed Aluminum-silver Excitation source. *J. Electron Spectrosc. Relat. Phenom.* **1990**, *50*, 159–166.

(42) Marcus, R. A. Chemical and Electrochemical Electron-Transfer Theory. *Annu. Rev. Phys. Chem.* **1964**, *15*, 155–196.

(43) Li, L. S.; Hu, J. T.; Yang, W. D.; Alivisatos, A. P. Band Gap Variation of Size- and Shape-controlled Colloidal CdSe Quantum Rods. *Nano Lett.* **2001**, *1*, 349–351.

(44) Khare, A.; Wills, A. W.; Ammerman, L. M.; Norris, D. J.; Aydil, E. S. Size Control and Quantum Confinement in Cu₂ZnSnS₄ Nanocrystals. *Chem. Commun.* **2011**, *47*, 11721–11723.

(45) Kongkanand, A.; Tvrđy, K.; Takechi, K.; Kuno, M.; Kamat, P. V. Quantum Dot Solar Cells. Tuning Photoresponse through Size and Shape Control of CdSe–TiO₂ Architecture. *J. Am. Chem. Soc.* **2008**, *130*, 4007–4015.

(46) van de Krol, R.; Grätzel, M. In *Photoelectrochemical Hydrogen Production*; van de Krol, R., Grätzel, M., Eds.; Springer: Boston, MA, 2012.

(47) Bae, D.; Seger, B.; Vesborg, P. C. K.; Hansen, O.; Chorkendorff, I. Strategies for Stable Water Splitting via Protected Photoelectrodes. *Chem. Soc. Rev.* **2017**, *46*, 1933–1954.

(48) Goto, Y.; Hisatomi, T.; Wang, Q.; Higashi, T.; Ishikiriya, K.; Maeda, T.; Sakata, Y.; Okunaka, S.; Tokudome, H.; Katayama, M.; Akiyama, S.; Nishiyama, H.; Inoue, Y.; Takewaki, T.; Setoyama, T.; Minegishi, T.; Takata, T.; Yamada, T.; Domen, K. A Particulate Photocatalyst Water-Splitting Panel for Large-Scale Solar Hydrogen Generation. *Joule* **2018**, *2*, 509–520.